Effects of ultrasound, radial extracorporeal shock waves, and electrical stimulation on rat bone defect healing

Inoue, Shota ; Hatakeyama, Junpei ; Aoki, Hitoshi ; Kuroki, Hiroshi ; Niikura, Takahiro ; Oe, Keisuke ; Fukui, Tomoaki ; Kuroda, Ryosuke ;…

Effects of ultrasound, radial extracorporeal shock wave, and electrical stimulation on rat bone defect healing

Short title: Effects of Physical Agents on bone defect healing

Shota Inoue [1], Junpei Hatakeyama [1], Hitoshi Aoki [2], Hiroshi Kuroki [3], Takahiro Niikura [4], Keisuke Oe [4], Tomoaki Fukui [4], Ryosuke Kuroda [4], Toshihiro Akisue [5], Hideki Moriyama [5*]

[1] Department of Rehabilitation Science, Graduate School of Health Sciences, Kobe University, Kobe, Japan

[2] OG Wellness Technologies Co., Ltd., Okayama, Japan

[3] Department of Physical Therapy, Human Health Sciences, Graduate School of Medicine, Kyoto University, Kyoto, Japan

[4] Department of Orthopaedic Surgery, Kobe University Graduate School of Medicine, Kobe, Japan

[5] Life and Medical Sciences Area, Health Sciences Discipline, Kobe University, Kobe, Japan

[*]**Correspondence:**

Hideki MORIYAMA, Ph.D.

Professor

Life and Medical Sciences Area, Health Sciences Discipline, Kobe University

Tomogaoka 7-10-2, Suma-ku, Kobe, Hyogo, 654-0142, Japan

Tel & Fax +81 78 796 4574

E-mail morihide@harbor.kobe-u.ac.jp

1   **Abstract**

2   Fractures associated with osteoporosis are major public health concerns. Current treatments

3   for fractures are limited to surgery or fixation, leading to long-term bedrest which is linked

4   to increased mortality. Alternatively, utilization of physical agents has been suggested as a

5   promising therapeutic approach for fractures. Here, we examined the effects of ultrasound,

6   radial extracorporeal shock waves, and electrical stimulation on normal or osteoporotic

7   fracture healing. Femoral bone defects were created in normal or ovariectomized rats. Rats

8   were divided into four groups: untreated, and treated with ultrasound, shock wave, or

9   electrical stimulation after surgery. Samples were collected at 2 or 4 weeks after surgery, and

10 the healing process was evaluated with micro-CT, histological, and immunohistochemical

11 analyses. Ultrasound at intensities of 0.5 and 1.0 W/cm^2, but not 0.05 W/cm^2, accelerated the

12 new bone formation. Shock wave exposure also increased the newly formed bone, but

13 formed the abnormal periosteal callus around the defect site. Conversely, electrical

14 stimulation did not affect the healing process. Ultrasound exposure increased osteoblast

15 activity and cell proliferation and decreased sclerostin-positive osteocytes. We demonstrated

16 that higher intensity ultrasound and radial extracorporeal shock wave accelerate fracture

17 healing, but shock wave treatment may increase risk of periosteal callus formation.

18

19 **Keywords** Ultrasound; Radial extracorporeal shock wave; Electrical stimulation; Fracture

20 healing

Introduction

Osteoporosis is characterized by low bone mass and poor bone microarchitecture, leading to a higher fracture susceptibility.[1] Current treatments for fractures involve surgery or fixation, resulting in prolonged bedrest; however, the long-term bedrest following fractures is linked to increased incidences of pulmonary embolism and heart failure,[2,3] and even mortality.[4] Therefore, novel treatment strategies are needed to accelerate fracture healing. We believe that one such promising treatment might be physical agents: ultrasound, radial extracorporeal shock wave, and electrical stimulation.

Among of the physical agents, low-intensity pulsed ultrasound (LIPUS) is the most widely prescribed for fracture healing.[5] However, accumulating recent evidence has shown the lack of LIPUS efficacy,[6–8] justifying the search for more effective physical agents and for optimal stimulation parameters to maximize the potential of physical agents for accelerating fracture healing.

To our current knowledge, no *in vivo* studies have investigated the biological effects of different physical agents on fracture healing. Furthermore, although it has been generally accepted that postmenopausal estrogen deficiency affects fracture healing process,[9–11] most *in vivo* studies of physical agents have focused on a single stimulation intensity or animal model.[12–22] We hypothesized that physical agents accelerate fracture healing and the responses to the physical agents can differ by its type and stimulation intensity. Hence, the present study aimed to verify the effects of three physical agents (ultrasound, radial extracorporeal shock waves, and electrical stimulation) with various intensities on fracture healing processes in normal or osteoporotic rats. The goal of our study was to develop novel and more effective therapeutic approaches for fractures utilizing physical agents, as an alternative to conventional treatments.

46 **Materials and Methods**

47 *Experimental design and animal care*

48 The protocols for the experiments were approved by our institutional animal care and use

49 committee and according to the Kobe University Animal Experimentation Regulations

50 (approval number: P160607). Male (n = 56, 5-6 months old, 500-600 g) and female (n = 36,

51 5-6 months old, 250-350 g) Wistar retired breeder rats were purchased from Japan SLC

52 (Shizuoka, Japan). The animals were housed in pairs in polycarbonate cages with bedding

53 and were maintained under artificial conditions at a constant temperature of 22 ± 1 °C with

54 constant humidity of $55\% \pm 5\%$ and a 12-hour light-dark cycle. They were allowed free

55 access to standard food and water 24 hours a day.

56 　　　　We investigated the effects of the physical agents on fracture repair in two

57 experiments (normal and osteoporotic fracture models). In the study of the normal fracture

58 healing, male rats were anesthetized by intraperitoneal administration of 40 mg/kg sodium

59 pentobarbital, and bone defects 1.2 mm in diameter was created in mid-diaphysis region of

60 the bilateral femur as a reproducible and stable model of bone healing.[23–25] The defects

61 penetrated the cortex to the medullary cavity but did not penetrate the opposite cortex. Male

62 rats were chosen to avoid the effects of estrogen on bone turnover.[9] Then, the animals were

63 randomly divided into four groups: untreated after the bone defect creation (BD group) and

64 treated with ultrasound (BD + US group), radial extracorporeal shock wave (BD + rESW

65 group), or electrical stimulation (BD + ES group) after surgery (Fig. 1A). The physical agent

66 treatments for 1 week or 2 weeks with different stimulation intensity (0.05, 0.5, or 1.0

67 W/cm^2 for US group; 1, 2, or 4 bar for rESW group; 8 or 16 mA for ES group) were started

68 one day after surgery.

69 　　　　In the study of the osteoporotic fracture repair, female rats received bilateral

70 ovariectomy to simulate postmenopausal osteoporosis. After 8 weeks of ovariectomy, bone

71 defects 1.2 mm in diameter and 2.5 mm deep were created in the metaphysis of the bilateral

72 femurs (about 2 mm from the growth plate) of the rats as previously described.[26,27] Then, the

73 animals were randomly divided into four groups: untreated after the bone defect creation

74 (OVX-BD group) and treated with ultrasound (OVX-BD + US group), radial extracorporeal

75 shock wave (OVX-BD + rESW group), or electrical stimulation (OVX-BD + ES group) after

76 surgery (Fig. 1B). Starting from one day after the bone defect creation, the rats were treated

77 for 4 weeks with each physical agent with different stimulation intensity: 0.05, 0.5, or 1.0

78 W/cm^2 for US group; 1, 2, or 3 bar for rESW group; 8 or 16 mA for ES group.

79   All animals were euthanized by exsanguination under general anesthesia and

80 analgesia at the end of the experimental period. For the BD groups, the bilateral femurs were

81 harvested at 1 week for histological analyses (n = 3 limbs from 3 rats per group) or 2 weeks

82 for micro-computed tomography (μCT) and histological analyses (n = 4 limbs from 4 rats

83 per group). We used the left femurs for μCT analyses and the right femurs for histological

84 analyses. The histological and biomechanical changes were assessed only in the BD and BD

85 + US groups. For the OVX-BD group, the bilateral femurs were harvested at 12 weeks, and

86 we used the left femurs for μCT and biomechanical analyses (n = 4 limbs from 4 rats per

87 group) and the right femurs for histological analyses (n = 4 limbs from 4 rats per group).

88

89 *Ultrasound*

90 The animals received daily 20-min ultrasound exposure for 1 week or 2 weeks (BD + US

91 group) or 4 weeks (OVX-BD + US group) after the bone defect creation. Bilateral hindlimbs

92 of each rat were shaved and the ultrasound gel was applied. A plane circular transducer, 3.7

93 cm in diameter, with ultrasound device (SONICCTIZER, MINATO Medical Science Co.,

94 Ltd., Osaka, Japan) was then positioned over the experimental wound of each hindlimb,

95 while the animals were under general anesthesia. The device work at 20% duty cycle from 1

96   kHz of a pulse repetition frequency and generates a sine wave at 1.0 MHz with the LIPUS

97   intensity (spatial-averaged temporal-averaged intensity [I_{SATA}] = 0.05 W/cm^2) or the higher

98   intensity than LIPUS which minimizes thermal effects (I_{SATA} = 0.5 or 1.0 W/cm^2). [28]

99

100 *Radial extracorporeal shock wave*

101 The rats were treated with radial extracorporeal shock wave only once (BD + rESW group)

102 or four times of one weekly session (OVX-BD + rESW group). Both hind legs of the rats

103 were shaved, and a 15 mm-diameter probe was used and positioned over the experimental

104 wound of each hindlimb which applied an ultrasonic gel, while the animals were under

105 general anesthesia. The probe was connected to the radial shock wave device (Physio-

106 ShockMaster, SAKAI Medical Co., Ltd., Tokyo, Japan) and each femur was exposed to

107 radial pressure waves which consisted in a total of 2,000 shock waves per one session, at 5

108 Hz with three different intensities of 1, 2, or 4 bar for the BD + rESW group or 1, 2, or 3 bar

109 for the OVX-BD + rESW group.

110

111 *Electrical stimulation*

112 The rats received electrical stimulation daily for 10 min per day, for 2 weeks (BD + ES

113 group) or 4 weeks (OVX-BD + ES group) after the bone defect creation. Both hind legs of

114 the rats were shaved, and the rats were anesthetized. The bilateral quadriceps were then

115 electrically stimulated by paired gold surface electrodes 7 mm in diameter. The electrodes

116 were connected to an electrical stimulator (ASPIA TS-1000; Nihon Medix, Chiba, Japan) to

117 transmit a square pulse at a frequency of 10 Hz and a rest-insertion period of 1 s contraction

118 followed by 4 s rest with two different intensities of 8 or 16 mA.

119

120 *Micro-computed tomography (μCT)*

121 Cross-sectional scans were made at the drilled sites in each femur sample using micro three-

122 dimensional (3D) X-ray CT system (R_mCT2; Rigaku, Tokyo, Japan) with an isotropic

123 voxel resolution of 20 µm was employed at a voltage 90 kV and current 160 µA. The

124 scanned data were reconstructed by image analysis software (TRI/3D-BON; Ratoc, Tokyo,

125 Japan). For the quantification of the newly formed bone, the regions of interest (ROI) with a

126 cube ($750 \times 750 \times 750$ µm^3) were placed into the central bone defect area. Thresholds value

127 of 690 HA/mg^3 for the diaphyseal defects in the BD groups to define cortical bone[29] or 184

128 HA/mg^3 for the metaphyseal defects in the OVX-BD groups to define total bone including

129 cortical and trabecular bone[30] were used to define the newly formed bone which

130 characterized by bone volume fraction (BV/TV), trabecular number (Tb.N), trabecular

131 thickness (Tb.Th), and trabecular separation (Tb.Sp).

132

133 *Biomechanical testing*

134 The mechanical properties of the bone defect sites were assessed by an indentation test as

135 previously described.[31] The femurs were placed on the base fixed in a mechanical testing

136 machine (AUTOGRAPH, Shimadzu, Kyoto, Japan). A cylindrical indenter of 1.0 mm in

137 diameter was applied to the center of the bone defect at a constant displacement velocity of 1

138 mm/min. The indenter was allowed to penetrate the medullary cavity. The maximum load

139 was obtained from the load-deflection curve and determined as the strength of the newly

140 formed bone in the defect area. The biomechanical test in the OVX-BD + rESW group could

141 not be carried out because of the difficulty of visual confirmation of the metaphyseal defect

142 site due to the presence of diffuse fracture callus around the defects.

143

144 *Histology*

145 *Histological preparation*

146   Non-demineralized frozen sections were prepared according to the method described by

147   Kawamoto.[32] Briefly, the femur was freeze-embedded with super cryoembeding medium

148   (SCEM, Leica Microsystems, Tokyo, Japan) in isopentane at -75 °C. Cross-sections of the

149   femur in the coronal plane (5 µm thick) were cut from each sample and were then used for

150   histological or immunohistochemical analyses.

151

152   *Histological analysis*

153   For general histological studies, frozen sections were stained with von Kossa, safranin O/fast

154   greens, alkaline phosphatase (ALP), or tartrate-resistant acid phosphatase (TRAP)

155   (TRAP/ALP stain kit®; FUJIFILM Wako Pure Chemical, Tokyo, Japan), according to the

156   manufacturers' instructions. For histomorphometric analysis of ALP and TRAP staining,

157   two random field of view per sample were randomly taken from the bone defect regions with

158   a light microscope (BX53; Olympus, Tokyo, Japan) and a camera (DP73; Olympus) at a

159   magnification of 20X. Osteoblast surface was measured manually using Image J 1.50

160   (National Institutes of Health, Bethesda, MD, USA) as the total length of ALP-positive

161   surface divided by bone surface. Osteoclast surface was similarly analyzed following TRAP

162   staining.

163

164   *Immunohistochemistry*

165   Following the protocols in our laboratory,[33] the tissue sections were immunostained using

166   against sclerostin (diluted 1:800; AF1589, R&D Systems, Minneapolis, MN, USA) or

167   proliferating cell nuclear antigen (PCNA; 1:1500, D3H8P, Cell Signaling Technology,

168   Danvers, MA, UA). Immunoreactivity was visualized with diaminobenzidine

169   tetrahydrochloride reagent (ImmPACT[TM] DAB peroxidase substrate kit, SK-410, Vector

170   Lab., Burlingame, CA, USA). Then, the sections were counterstained Mayer's hematoxylin

171 for sclerostin or hematoxylin for PCNA. The immunolabeled sections were captured with the

172 light microscope (BX-53; Olympus) and the camera (DP73; Olympus) at a magnification of

173 20X. For sclerostin, the number of sclerostin-positive and total osteocytes were manually

174 counted in two random regions of the cortical bone around the bone defect area per sample.

175 For PCNA, the number of immune-positive cells was manually counted in one random fields

176 of view in the bone defect regions per sample.

177

178 *Statistical analysis*

179 Statistical analyses were conducted with EZR (Saitama Medical Center, Jichi Medical

180 University, Saitama, Japan), which is a graphical user inter face for R (The R Foundation for

181 Statistical Computing, Vienna, Austria).[34] First, all data were checked for normality with the

182 Shapiro-Wilk test. Normality was observed in all analyses, and the results were compared

183 among groups with the one-way ANOVA test followed by the Tukey HSD test. All values

184 are presented here as mean ± standard deviation (SD). *P* values less than 0.05 were

185 considered significant. A post hoc power analysis was used to confirm that sufficient number

186 of animals had been used.

187

188 **Results**

189 *Morphologic changes in diaphyseal defect*

190 3D reconstructions of the newly formed bone in the diaphyseal defects showed that the rats

191 treated with ultrasound at 0.5 and 1.0 W/cm^2 had more new bone than untreated rats (Fig.

192 2A). This was confirmed by increased BV/TV and Tb.N in the 0.5 and 1.0 W/cm^2 US-

193 treated groups compared to the BD group ($P < 0.05$, power = 1.00) (Fig. 2B and

194 Supplementary Table 1). Furthermore, representative histological evidence of bone

195 mineralization supported the findings obtained by μCT analysis (Fig. 2C). The newly formed

196 bone across the cortical gap was thicker and denser in the 0.5 and 1.0 W/cm^2 US-treated

197 groups compared to the untreated group.

198

199 *Morphologic changes in metaphyseal defect*

200 Representative images in the femoral metaphyseal defect sites revealed that the defects in the

201 OVX-BD + US and rESW groups, except for the US group at 0.05 W/cm^2, were filled with

202 the newly formed bone compared to the OVX-BD group (Fig. 3A). Von Kossa staining

203 showed that these groups had the more abundant bone in the defect sites than the OVX-BD

204 group (Fig. 3B). Quantitative measurements of the newly formed bone with µCT analyses

205 revealed that BV/TV increased in the rats treated with ultrasound at 1.0 W/cm^2 or

206 extracorporeal shock wave at 1, 2, and 3 bar when compared to the untreated rats ($P < 0.05$,

207 power = 1.00) (Fig. 3C). Furthermore, in the 1.0 W/cm^2 US-treated group, BV/TV was

208 larger than in the 0.05 W/cm^2 US-treated group ($P < 0.05$). These findings were reinforced

209 by the other structural parameters by µCT analyses (Supplementary Table 2). On the other

210 hand, in the rats that received radial extracorporeal shock wave, the periosteal callus was

211 observed near the defect site in the 3D images by µCT (Fig. 3A), histological sections (Fig.

212 3B and 3D, left), and macroscopic observation (Fig. 3D, right).

213

214 *Biomechanical properties*

215 The biomechanical strength of the new bone in the defect sites which was determined by the

216 maximum load showed no differences between the untreated and treated groups both in the

217 normal and osteoporotic rats.

218

219 *Osteoblast and osteoclast activity*

220   In the diaphyseal defects, ALP-positive regions increased in the 0.5 and 1.0 W/cm^2 US-

221   treated groups compared to the untreated ($P < 0.05$, power = 0.96) (Fig. 4A, top and B).

222   TRAP staining revealed the localization of osteoclast in the diaphyseal defects at 7 days after

223   surgery (Fig. 4A, bottom). There was no significant change in the percentage of osteoclast

224   surface among all groups (power = 0.95) (Fig. 4C).

225   In the metaphyseal defects, ALP-stained bone surfaces in the OVX-BD + rESW and

226   US at 1.0 W/cm^2 were higher than OVX-BD group (P < 0.05, power = 1.00) (Fig. 5A and

227   B). TRAP-positive regions were observed in all groups (Fig. 5C), but there were no

228   significant differences in the percentage of osteoclast surface among all groups (power =

229   1.00) (Fig. 5D).

230

231   *Immunohistochemical pattern of sclerostin and PCNA*

232   The sclerostin-positive osteocytes around the defect area were tended to decreased in the 1.0

233   W/cm^2 US-treated group (versus untreated, $P = 0.09$, power = 0.96) (Fig. 6A, top and Table

234   2). In the metaphyseal defects, the percentage of sclerostin-positive osteocytes decreased in

235   the OVX-BD + US at 1.0 W/cm^2 and rESW groups when compared to the OVX-BD group

236   ($P < 0.05$, power = 1.00).

237   In the BD + US at 0.5 and 1.0 W/cm^2 groups, PCNA-positive cells were densely

238   distributed in the bone marrow at the defect area when compared to the untreated group at 7

239   days after the surgery (Fig. 6, bottom). The number of PCNA-positive cells increased in the

240   0.5 and 1.0 W/cm^2 US-treated group ($P < 0.05$, power = 0.97) (Table 2).

241

242   **Discussion**

243   This study investigated the effects of ultrasound, radial extracorporeal shock wave, and

244   electrical stimulation on normal or osteoporotic fracture healing in rat bone defect models.

245 As a result, ultrasound at higher intensity (0.5 and 1.0 W/cm^2) accelerated normal fracture

246 healing, but not radial extracorporeal shock wave and electrical stimulation. We found that

247 high intensity ultrasound exposure increased cell proliferation and osteoblast activity at the

248 healing site. The results in the osteoporotic fracture model showed that ultrasound at higher

249 intensity (1.0 W/cm^2) and radial extracorporeal shock wave accelerate fracture healing under

250 estrogen-deficient conditions. However, we also found that shock wave treatment may

251 increase risk of the abnormal periosteal callus formation.

252 Based on the μCT analyses, ultrasound at intensity 0.05 W/cm^2 did not affect the

253 new bone formation in the bone defect both in the normal and osteoporotic rats. This accords

254 with previous clinical[7,8] and animal reports,[35–37] showing no stimulatory effect of LIPUS at

255 intensity less than 0.1 W/cm^2 on fracture healing processes. Meanwhile, ultrasound at higher

256 intensity (0.5 or 1.0 W/cm^2) than LIPUS accelerated bone formation at the bone defect site

257 both in the normal and osteoporotic rats. These are similar to the report that ultrasound at

258 intensity 0.3 W/cm^2 accelerated bone formation in the bone defect, but not at intensity 0.1

259 W/cm^2.[35] Moreover, ultrasound exposure at various intensities ranging from 0.015 to 0.15

260 W/cm^2 [38] or 0.005 to 0.1 W/cm^2 [39] improved estrogen-deficient bone loss in an intensity-

261 dependent manner. In line with these previous findings, our results indicate that ultrasound

262 exposure at higher intensity than LIPUS enhances bone formation both in normal and

263 osteoporotic fracture healing. Although high intensity ultrasound can induce some side

264 effects such as skin necrosis at 2.5 W/cm^2 [40] and osteonecrosis with increased bone

265 resorption at 2.2 W/cm^2 [41], the rats treated with ultrasound at 0.5 and 1.0 W/cm^2 had no

266 gross, physical, or histological abnormalities. Consequently, these findings suggest the

267 possibility that higher intensity ultrasound than LIPUS is a promising noninvasive treatment

268 for fracture healing.

269   Consistent with previous reports showing the effectiveness of focused

270   extracorporeal shock wave in fracture healing,[15,16,42,43] radial extracorporeal shock wave

271   increased the newly formed bone in the osteoporotic fracture model. Furthermore, the shock

272   wave at all three intensities (1, 2, and 3 bar) increased the newly formed bone, indicating that

273   this treatment can accelerate osteoporotic fracture healing, irrespective of the stimulation

274   intensity. Although radial shock waves have the advantage of being lower energy and less

275   pain for patients than focused shock waves, in this study, its exposure also induced the

276   diffuse callus formation around the bone defect. In the metaphyseal defect model, a small

277   amount of the periosteal callus is observed during the healing process, and its formation

278   peaks at day 14 and is completely resorbed at day 28 to 35 after the defect creation.[44]

279   Meanwhile, the callus induced by the shock wave still remained in the defect site at 4 weeks

280   after surgery and was greater than that of the untreated rats, implying the abnormal bone

281   healing process. Taken together, these findings indicate that radial extracorporeal shock

282   wave in one weekly session accelerate osteoporotic fracture healing, but its treatment may

283   potentially increase the abnormal callus formation.

284   Ultrasound and radial extracorporeal shock wave accelerated fracture healing, while

285   muscle contraction induced by electrical stimulation did not affect the new bone formation in

286   both normal and osteoporotic fractures. This is inconsistent with a previous animal study

287   showing that the electrically-induced muscular contraction enhances fracture healing in

288   rabbits.[22] Although the defect area is filled with the hematoma and fibrous tissue rapidly

289   after surgery,[24] the bone defect may be less likely to respond to longitudinal stress induced

290   by muscular contraction than the transverse fracture. Thus, muscle contraction induced by

291   electrical stimulation may be insufficient to affect bone defect healing.

292   We evaluated the mechanical strength of the newly formed bone at the defect sites

293   using the indentation test, which has been widely used in measuring the biomechanical

294 properties of bone in different experimental conditions.[31] As a consequence, ultrasound

295 exposure at higher intensity had no effect on maximum load in normal and osteoporotic rats,

296 despite increased new bone mass at the defect site. The bone strength is determined not only

297 by the quantity of bone tissue but also by its quality, which is characterized by the trabecular

298 microarchitecture, the mineral and collagen, and the shape of bones.[45] Whether ultrasound

299 exposure affects the bone quality is unclear in this study, but our results indicate that its

300 exposure for 2 or 4 weeks does not affect the bone strength at the healing site.

301   Bone defect healing occurs mainly through intramembranous ossification via direct

302 differentiation of osteoblasts from mesenchymal cells in the initial phase of the healing

303 process.[24] Ultrasound at 0.5 and 1.0 W/cm^2 increased ALP activity, a differentiation marker

304 of osteoblasts,[46] in the normal fracture model at the initial phase of defect healing (7 days

305 after surgery). In the osteoporotic rats, ultrasound at 1.0 W/cm^2 and radial extracorporeal

306 shock waves at 1 and 3 bar also enhanced its activity at the later phase (4 weeks after

307 surgery), implying that these treatments could activate osteoblasts both in the initial and later

308 phases of healing processes. In addition, high intensity ultrasound and shock wave were

309 tended to decrease sclerostin-positive osteocytes, paralleled by increased osteoblast activity.

310 Sclerostin inhibits the osteoblast differentiation and activity by antagonizing Wnt/β catenin

311 signaling.[47] Additionally, sclerostin deficient mice enhances intramembranous ossification of

312 bone defects by increasing the β-catenin expression and osteoblast number.[48] Thus, these

313 findings suggest that higher intensity ultrasound and radial extracorporeal shock wave

314 activate osteoblasts, at least in part, via downregulation of sclerostin in osteocytes, thereby

315 accelerating bone healing.

316   Cell proliferation is essential for fracture healing processes, particularly in the early

317 stages of the healing.[49,50] Consistent with the previous reports,[14,51–53] ultrasound at intensity

318 0.05 W/cm^2 did not affect the number of PCNA-positive cells, a marker of cell

319 proliferation[54], at the early phase of defect healing (7 days after surgery). In contrast,

320 ultrasound at 0.5 and 1.0 W/cm^2 enhanced cell proliferation at the same time point, as

321 indicated by increased PCNA-positive cells at the bone defect site. This corresponds to the

322 report that high magnitude strain in the physiological range stimulates cell proliferation of

323 bone marrow stromal cells.[55] Collectively, these findings suggest that higher intensity

324 ultrasound enhanced cell proliferation, in addition to osteoblast differentiation, leading to

325 accelerated fracture healing.

326   This study had several limitations. The differences in sex, age, and the defect site

327 make it difficult to compare the results between normal and osteoporotic rats. Therefore, we

328 cannot conclude from the present study whether the response of physical agents differed

329 with or without estrogen. In addition, we could not examine the effects of physical agents on

330 endochondral ossification. The bone defect model has been used in many studies of fracture

331 healing as a reproducible and stable model.[23–27] This model is healed only by

332 intramembranous ossification,[56] while transverse fracture healing in humans occurs through

333 not only intramembranous but also endochondral ossification.[57] Our study showed that the

334 physical agents enhanced intramembranous ossification, but their stimulatory effect on

335 endochondral ossification cannot at present be answered. Therefore, further research should

336 explore the safety and efficacy of physical agents in clinical trials and animal studies with

337 transverse fractures.

338   In conclusion, we demonstrated that higher intensity ultrasound than LIPUS

339 accelerates both normal and osteoporotic fracture healing. Our findings also showed that

340 radial extracorporeal shock wave enhances osteoporotic fracture healing, but its treatment

341 may increase risk of the abnormal periosteal callus formation. Future studies are needed to

342 determine if our findings are clinically applicable.

343

Acknowledgments

Competing interests

The authors declare no competing interests.

356 **Reference**

357   1.   NIH Consensus Development Panel on Osteoporosis Prevention, Diagnosis. and

358   Therapy 2001. Osteoporosis prevention, diagnosis, and therapy. *JAMA* **285**: 785–795.

359   2.   Wehren L.E., W.G. Hawkes, D.L. Orwig, *et al.* 2003. Gender Differences in Mortality

360   after Hip Fracture: The Role of Infection. *J. Bone Miner. Res.* **18**: 2231–2237.

361   3.   Roche J.J.W., R.T. Wenn, O. Sahota, *et al.* 2005. Effect of comorbidities and

362   postoperative complications on mortality after hip fracture in elderly people:

363   Prospective observational cohort study. *Br. Med. J.* **331**: 1374–1376.

364   4.   Vestergaard P., L. Rejnmark & L. Mosekilde. 2007. Increased mortality in patients

365   with a hip fracture-effect of pre-morbid conditions and post-fracture complications.

366   *Osteoporos. Int.* **18**: 1583–1593.

367   5.   Watanabe Y., T. Matsushita, M. Bhandari, *et al.* 2010. Ultrasound for Fracture

368   Healing: Current Evidence. *J. Orthop. Trauma* **24**: S56–S61.

369   6.   Lou S., H. Lv, Z. Li, *et al.* 2018. Effect of low-intensity pulsed ultrasound on

370   distraction osteogenesis: A systematic review and meta-analysis of randomized

371   controlled trials. *J. Orthop. Surg. Res.* **13**: 1–10.

372   7.   Busse J.W., M. Bhandari, T.A. Einhorn, *et al.* 2016. Re-evaluation of low intensity

373   pulsed ultrasound in treatment of tibial fractures (TRUST): Randomized clinical trial.

374   *BMJ* **355**: i5351.

375   8.   Schandelmaier S., A. Kaushal, L. Lytvyn, *et al.* 2017. Low intensity pulsed ultrasound

376   for bone healing: systematic review of randomized controlled trials. *BMJ* **356**: j656.

377   9.   McCann R.M., G. Colleary, C. Geddis, *et al.* 2008. Effect of osteoporosis on bone

378   mineral density and fracture repair in a rat femoral fracture model. *J. Orthop. Res.* **26**:

379   384–393.

380   10.   Namkung-Matthai H., R. Appleyard, J. Jansen, *et al.* 2001. Osteoporosis influences

381   the early period of fracture healing in a rat osteoporotic model. *Bone* **28**: 80–86.

382   11.   Lill C.A., J. Hesseln, U. Schlegel, *et al.* 2003. Biomechanical evaluation of healing in

383   a non-critical defect in a large animal model of osteoporosis. *J. Orthop. Res.* **21**: 836–

384   842.

385   12.   Azuma Y., M. Ito, Y. Harada, *et al.* 2001. Low-intensity pulsed ultrasound accelerates

386   rat femoral fracture healing by acting on the various cellular reactions in the fracture

387   callus. *J. Bone Miner. Res.* **16**: 671–680.

388   13.   Cheung W.-H., W.-C. Chin, L. Qin, *et al.* 2012. Low intensity pulsed ultrasound

389   enhances fracture healing in both ovariectomy-induced osteoporotic and age-matched

390   normal bones. *J. Orthop. Res.* **30**: 129–136.

391   14.   Gebauer G.P., S.S. Lin, H.A. Beam, *et al.* 2002. Low-intensity pulsed ultrasound

392   increases the fracture callus strength in diabetic BB Wistar rats but does not affect

393   cellular proliferation. *J. Orthop. Res.* **20**: 587–592.

394   15.   Wang C.J., K.D. Yang, F.S. Wang, *et al.* 2004. Shock wave treatment shows dose-

395   dependent enhancement of bone mass and bone strength after fracture of the femur.

396   *Bone* **34**: 225–230.

397   16.   Chen X.F., H.M. Huang, X.L. Li, *et al.* 2015. Slightly focused high-energy

398   shockwave therapy: a potential adjuvant treatment for osteoporotic fracture. *Int. J.*

399   *Clin. Exp. Med.* **8**: 5044–54.

400   17.   van der Jagt O.P., T.M. Piscaer, W. Schaden, *et al.* 2011. Unfocused Extracorporeal

401   Shock Waves Induce Anabolic Effects in Rat Bone. *J. Bone Jt. Surgery-American*

402   *Vol.* **93**: 38–48.

403 18. Van Der Jagt O.P., J.C. Van Der Linden, W. Schaden, *et al.* 2009. Unfocused

404   extracorporeal shock wave therapy as potential treatment for osteoporosis. *J. Orthop.*

405   *Res.* **27**: 1528–1533.

406 19. Van Der Jagt O.P., J.H. Waarsing, N. Kops, *et al.* 2013. Unfocused extracorporeal

407   shock waves induce anabolic effects in osteoporotic rats. *J. Orthop. Res.* **31**: 768–775.

408 20. Özkan E., M.C. Bereket, M.E. Önger, *et al.* 2018. The effect of unfocused

409   extracorporeal shock wave therapy on bone defect healing in diabetics. *J. Craniofac.*

410   *Surg.* **29**: 1081–1086.

411 21. Koolen M.K.E., B. Pouran, F.C. Öner, *et al.* 2018. Unfocused shockwaves for

412   osteoinduction in bone substitutes in rat cortical bone defects. *PLoS One* **13**:

413   e0200020.

414 22. Park S.H. & M. Silva. 2004. Neuromuscular electrical stimulation enhances fracture

415   healing: Results of an animal model. *J. Orthop. Res.* **22**: 382–387.

416 23. Chen Y.J., Y.R. Kuo, K.D. Yang, *et al.* 2004. Activation of extracellular signal-

417   regulated kinase (ERK) and p38 kinase in shock wave-promoted bone formation of

418   segmental defect in rats. *Bone* **34**: 466–477.

419 24. Chiba S., K. Okada, K. Lee, *et al.* 2001. Molecular Analysis of Defect Healing in Rat

420   Diaphyseal Bone. *J. Vet. Med. Sci.* **63**: 603–608.

421 25. Kim J.B., P. Leucht, K. Lam, *et al.* 2007. Bone regeneration is regulated by Wnt

422   signaling. *J. Bone Miner. Res.* **22**: 1913–1923.

423 26. Cheng N., J. Dai, X. Cheng, *et al.* 2013. Porous CaP/silk composite scaffolds to repair

424   femur defects in an osteoporotic model. *J. Mater. Sci. Mater. Med.* **24**: 1963–1975.

425 27. Zhang Y., N. Cheng, R. Miron, *et al.* 2012. Delivery of PDGF-B and BMP-7 by

426   mesoporous bioglass/silk fibrin scaffolds for the repair of osteoporotic defects.

427   *Biomaterials* **33**: 6698–6708.

428 28. Baker K.G., V.J. Robertson & F.A. Duck. 2001. A Review of Therapeutic Ultrasound:

429   Biophysical Effects. *Phys. Ther*. **81**: 1351–1358.

430 29. Tanaka M., A. Sakai, S. Uchida, *et al.* 2004. Prostaglandin E2 receptor (EP4)

431   selective agonist (ONO-4819.CD) accelerates bone repair of femoral cortex after drill-

432   hole injury associated with local upregulation of bone turnover in mature rats. *Bone*

433   **34**: 940–948.

434 30. Wei L., J. Ke, I. Prasadam, *et al.* 2014. A comparative study of Sr-incorporated

435   mesoporous bioactive glass scaffolds for regeneration of osteopenic bone defects.

436   *Osteoporos. Int.* **25**: 2089–2096.

437 31. Fangel R., P. Sérgio Bossini, A. Cláudia Renno, *et al.* 2011. Low-level laser therapy,

438   at 60 J/cm2 associated with a Biosilicate® increase in bone deposition and indentation

439   biomechanical properties of callus in osteopenic rats. *J. Biomed. Opt.* **16**: 078001.

440 32. Kawamoto T. 2003. Use of a new adhesive film for the preparation of multi-purpose

441   fresh-frozen sections from hard tissues, whole-animals, insects and plants. *Arch.*

442   *Histol. Cytol.* **66**: 123–43.

443 33. Moriyama H., N. Kanemura, I. Brouns, *et al.* 2012. Effects of aging and exercise

444   training on the histological and mechanical properties of articular structures in knee

445   joints of male rat. *Biogerontology* **13**: 369–381.

446 34. Kanda Y. 2013. Investigation of the freely available easy-to-use software "EZR" for

447   medical statistics. *Bone Marrow Transplant.* **48**: 452–8.

448 35. Lavandier B., A. Gleizal & J.C. Béra. 2009. Experimental Assessment of Calvarial

449   Bone Defect Re-Ossification Stimulation Using Low-Intensity Pulsed Ultrasound.

450   *Ultrasound Med. Biol.* **35**: 585–594.

451   36.   Lirani-Galvão A.P., V. Jorgetti & O. Lopes Da Silva. 2006. Comparative study of

452   how low-level laser therapy and low-intensity pulsed ultrasound affect bone repair in

453   rats. *Photomed. Laser Surg.* **24**: 735–740.

454   37.   Fávaro-Pípi E., S.M. Feitosa, D.A. Ribeiro, *et al.* 2010. Comparative study of the

455   effects of low-intensity pulsed ultrasound and low-level laser therapy on bone defects

456   in tibias of rats. *Lasers Med. Sci.* **25**: 727–732.

457   38.   Sun S., L. Sun, Y. Kang, *et al.* 2020. Therapeutic Effects of Low-Intensity Pulsed

458   Ultrasound on Osteoporosis in Ovariectomized Rats: Intensity-Dependent Study.

459   *Ultrasound Med. Biol.* **46**: 108–121.

460   39.   Ferreri S.L., R. Talish, T. Trandafir, *et al.* 2011. Mitigation of bone loss with

461   ultrasound induced dynamic mechanical signals in an OVX induced rat model of

462   osteopenia. *Bone* **48**: 1095–1102.

463   40.   Boucaud A., J. Montharu, L. Machet, *et al.* 2001. Clinical, histologic, and electron

464   microscopy study of skin exposed to low-frequency ultrasound. *Anat. Rec.* **264**: 114–

465   119.

466   41.   Lyon R., X.C. Liu & J. Meier. 2003. The effects of therapeutic vs. high-intensity

467   ultrasound on the rabbit growth plate. *J. Orthop. Res.* **21**: 865–871.

468   42.   Rompe J.D., T. Rosendahl, C. Schöllner, *et al.* 2001. High-energy extracorporeal

469   shock wave treatment of nonunions. *Clin. Orthop. Relat. Res.* 102–111.

470   43.   Kieves N.R., C.S. Mackay, K. Adducci, *et al.* 2015. High energy focused shock wave

471   therapy accelerates bone healing: A blinded, prospective, randomized canine clinical

472   trial. *Vet. Comp. Orthop. Traumatol.* **28**: 425–432.

473   44.   Inoue S., H. Otsuka, J. Takito, *et al.* 2018. Decisive differences in the bone repair

474   processes of the metaphysis and diaphysis in young mice. *Bone Reports* **8**: 1–8.

475 45. Viguet-Carrin S., P. Garnero & P.D. Delmas. 2006. The role of collagen in bone

476   strength. *Osteoporos. Int.* **17**: 319–336.

477 46. Rawadi G., B. Vayssière, F. Dunn, *et al.* 2003. BMP-2 Controls Alkaline Phosphatase

478   Expression and Osteoblast Mineralization by a Wnt Autocrine Loop. *J. Bone Miner.*

479   *Res.* **18**: 1842–1853.

480 47. Sapir-Koren R. & G. Livshits. 2014. Osteocyte control of bone remodeling: is

481   sclerostin a key molecular coordinator of the balanced bone resorption–formation

482   cycles? *Osteoporos. Int.* **25**: 2685–2700.

483 48. McGee-Lawrence M.E., Z.C. Ryan, L.R. Carpio, *et al.* 2013. Sclerostin deficient mice

484   rapidly heal bone defects by activating β-catenin and increasing intramembranous

485   ossification. *Biochem. Biophys. Res. Commun.* **441**: 886–890.

486 49. Li G., G. White, C. Connolly, *et al.* 2002. Cell Proliferation and Apoptosis During

487   Fracture Healing. *J. Bone Miner. Res.* **17**: 791–799.

488 50. Gerstenfeld L.C., D.M. Cullinane, G.L. Barnes, *et al.* 2003. Fracture healing as a post-

489   natal developmental process: Molecular, spatial, and temporal aspects of its

490   regulation. *J. Cell. Biochem.* **88**: 873–884.

491 51. Schumann D., R. Kujat, J. Zellner, *et al.* 2006. Treatment of human mesenchymal

492   stem cells with pulsed low intensity ultrasound enhances the chondrogenic phenotype

493   in vitro. *Biorheology* **43**: 431–443.

494 52. Lee S.Y., A. Koh, T. Niikura, *et al.* 2013. Low-Intensity Pulsed Ultrasound Enhances

495   BMP-7-Induced Osteogenic Differentiation of Human Fracture Hematoma-Derived

496   Progenitor Cells In Vitro. *J. Orthop. Trauma.* **27**: 29–33.

497 53. Kang K.S., S.J. Lee, H. Lee, *et al.* 2011. Effects of combined mechanical stimulation

498   on the proliferation and differentiation of pre-osteoblasts. *Exp. Mol. Med.* **43**: 367–

499   373.

500   54.   Muskhelishvili L., J.R. Latendresse, R.L. Kodell, *et al.* 2003. Evaluation of Cell

501   Proliferation in Rat Tissues with BrdU, PCNA, Ki-67(MIB-5) Immunohistochemistry

502   and in Situ Hybridization for Histone mRNA. *J. Histochem. Cytochem.* **51**: 1681–

503   1688.

504   55.   Koike M., H. Shimokawa, Z. Kanno, *et al.* 2005. Effects of mechanical strain on

505   proliferation and differentiation of bone marrow stromal cell line ST2. *J. Bone Miner.*

506   *Metab.* **23**: 219–225.

507   56.   Monfoulet L., B. Rabier, O. Chassande, *et al.* 2010. Drilled hole defects in mouse

508   femur as models of intramembranous cortical and cancellous bone regeneration.

509   *Calcif. Tissue. Int.* **86**: 72–81.

510   57.   Einhorn T.A. 2005. The science of fracture healing. *J. Orthop. Trauma.* **19**: 19–21.

511 **Figure legends**

512 **Fig. 1** (**A**) A Diagram of the experimental design for the studies of the normal fracture

513 healing is shown. The bilateral femurs were harvested at 1 week for histological analyses (n

514 = 3 limbs from 3 rats per group) or 2 weeks for µCT and histological analyses (n = 4 limbs

515 from 4 rats per group) and biomechanical testing (n = 4 limbs from 2 rats per group). We

516 used the right femurs for µCT analyses and the left femurs for histological analyses. (**B**) A

517 Diagram of the experimental design for the studies of the osteoporotic fracture healing is

518 shown. The bilateral femurs were harvested at 12 weeks, and we used the left femurs for

519 µCT and biomechanical analyses (n = 4 limbs from 4 rats per group) and the right femurs for

520 histological analyses (n = 4 limbs from 4 rats per group). OVX = ovariectomy; BD = bone

521 defect; US = ultrasound; rESW = radial extracorporeal shock wave; ES = electrical

522 stimulation

523

524 **Fig. 2** Morphologic changes in the diaphyseal defect of normal rats after 2 weeks of the

525 defect creation. (**A**) Representative 3D images show the newly formed bone at the

526 diaphyseal defect site obtained by µCT analysis. Scale bar = 500 µm. (**B**) The graph shows

527 quantification of the bone volume in the defect by µCT analysis (n = 4 femurs per group).

528 Data are expressed as mean ± SD. *$P < 0.05$ vs. BD group; †$P < 0.10$ vs. BD + US at 0.05

529 W/cm^2 group. (**C**) Representative histological images in the defect area stained with von

530 Kossa are shown. Scale bars = 500 µm. BD = bone defect; US = ultrasound; rESW = radial

531 extracorporeal shock wave; ES = electrical stimulation; BV/TV = bone volume/tissue

532 volume

533

534 **Fig. 3** Morphologic changes in the metaphyseal defect of osteoporotic rats after 4 weeks of

535 the defect creation. (**A**) Representative 3D images show the metaphyseal defect site obtained

536 by µCT analysis. Scale bar = 2 mm. (**B**) Representative histological images in the defect

537 stained with von Kossa are shown. Scale bars = 500 µm. (**C**) The graph shows quantification

538 of the bone volume in the defect by µCT analysis (n = 4 femurs per group). Data are

539 expressed as mean ± SD. *$P < 0.05$ vs. OVX-BD group; †$P < 0.05$ vs. OVX-BD + US at

540 0.05 W/cm^2 group. (**D**) Representative histological images in the distal femur stained with

541 safranin O/fast green (left) and macroscopic observations of the femur (right) are shown.

542 Arrowheads indicate the site of the defect creation. Scale bars = 1 mm (left) and 5 mm

543 (right). OVX = ovariectomy; BD = bone defect; US = ultrasound; rESW = radial

544 extracorporeal shock wave; ES = electrical stimulation; BV/TV = bone volume/tissue

545 volume

546

547 **Fig. 4** (**A**) Representative histological images in the diaphyseal defect sites of normal rats

548 after 1 week of the defect creation stained with ALP (top) and TRAP (bottom) are shown.

549 Scale bars = 100 µm. (**B**) The graphs show quantification of ALP staining by osteoblast

550 surface per bone surface (**C**) and TRAP staining by osteoclast surface per bone surface (n =

551 3 femurs per group). Data are expressed as mean ± SD. *$P < 0.05$ vs. BD group. BD = bone

552 defect; US = ultrasound

553

554 **Fig. 5** (**A**) Representative histological images in the metaphyseal defect sites of osteoporotic

555 rats after 4 weeks of the defect creation stained with ALP are shown. Scale bars = 100 µm.

556 (**B**) The graph shows quantification of ALP staining by osteoblast surface per bone surface

557 (n = 4 femurs per group). (**C**) Representative histological images in the metaphyseal defect

558 sites stained with TRAP are shown. Scale bars = 100 µm. (**D**) The graph shows

559 quantification of TRAP staining by osteoclast surface per bone surface (n = 4 femurs per

560 group). Data are expressed as mean ± SD. *$P < 0.05$ vs. OVX-BD group; †$P < 0.05$ vs.

561 OVX-BD + US at 0.05 W/cm^2 group; ‡P < 0.05 vs. OVX-BD + US at 0.5 W/cm^2 group.

562 OVX = ovariectomy; BD = bone defect; US = ultrasound; rESW = radial extracorporeal

563 shock wave; ES = electrical stimulation

564

565 **Fig. 6** Representative photomicrographs show the distribution of sclerostin in the cortical

566 bone around the diaphyseal defect area of normal rats after 2 weeks of the defect creation

567 (top). Representative photomicrographs show the distribution of PCNA in the diaphyseal

568 bone defect sites of normal rats after 1 week of the defect creation (bottom). Scale bars =
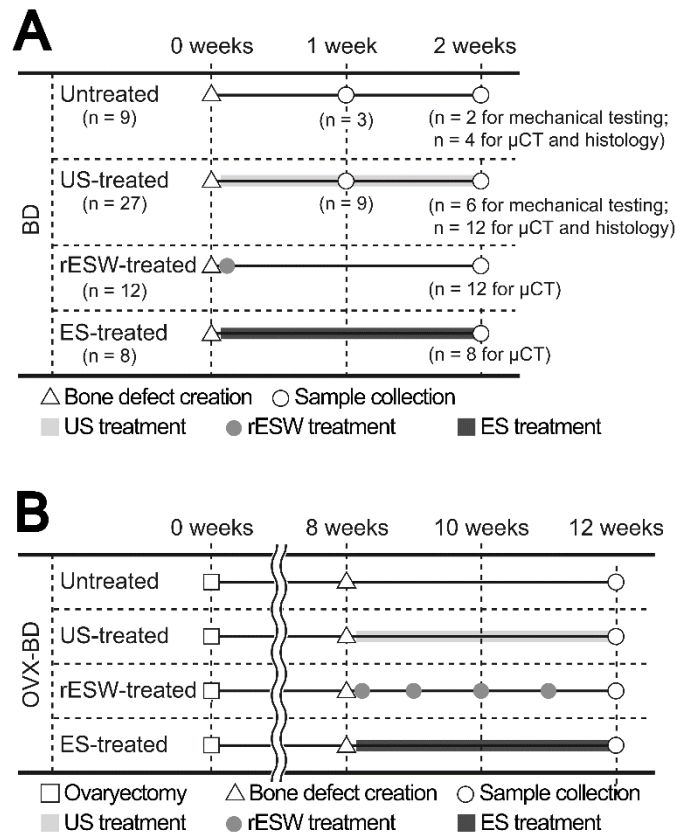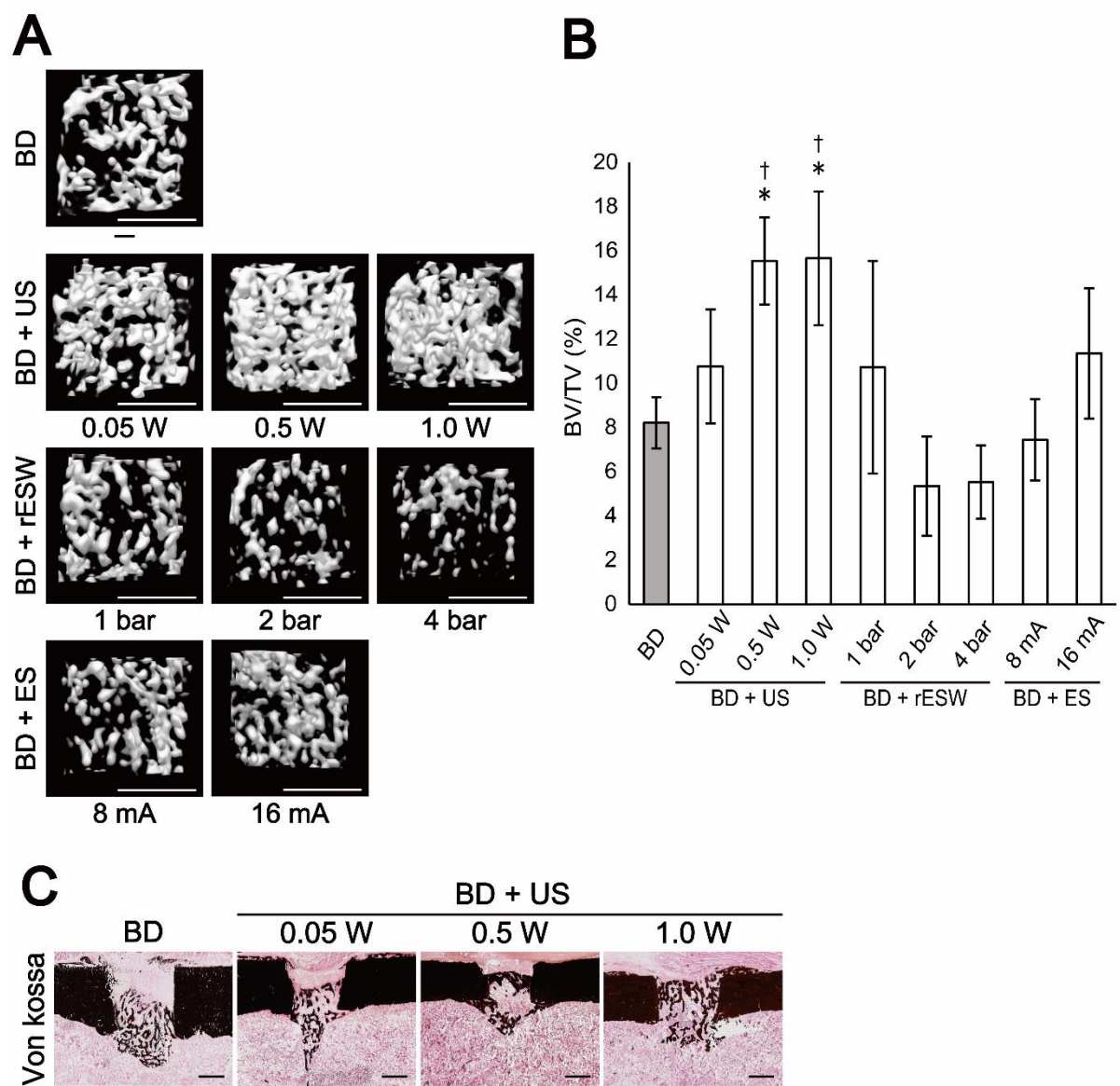
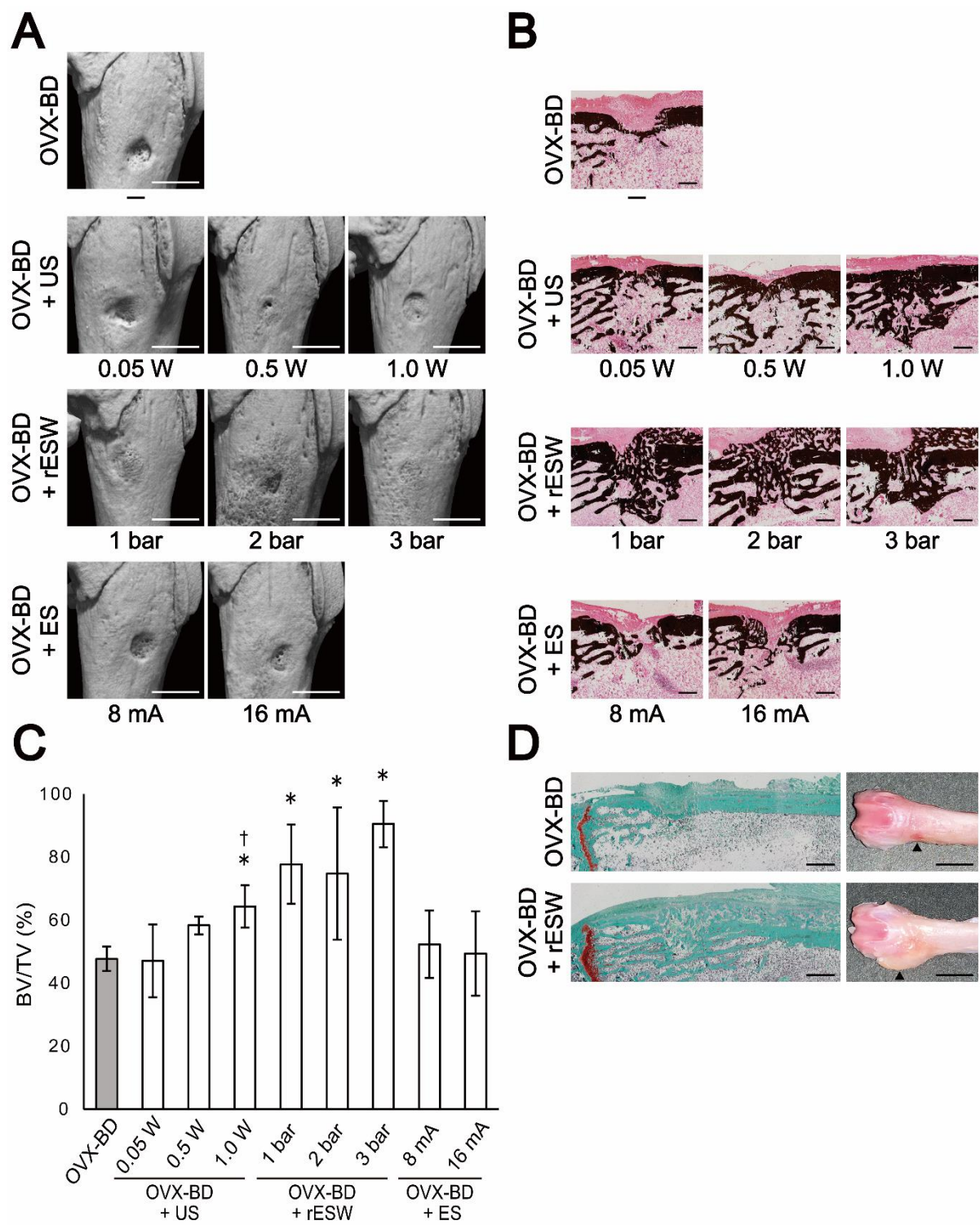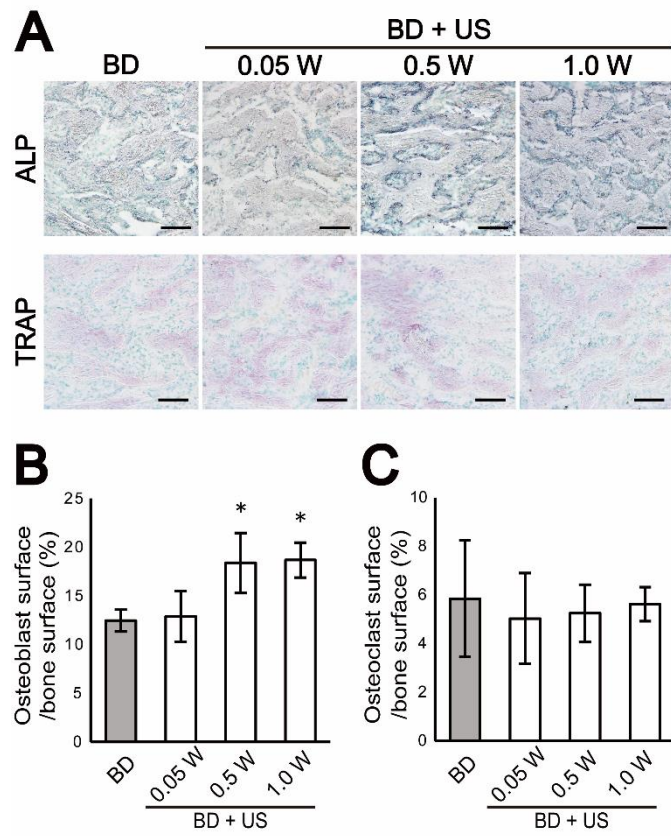569 100 µm. BD = bone defect; US = ultrasound

Figure 1

Figure 2

A

OVX-BD

OVX-BD + US
0.05 W   0.5 W   1.0 W

OVX-BD + rESW
1 bar   2 bar   3 bar

OVX-BD + ES
8 mA   16 mA

B

OVX-BD

OVX-BD + US
0.05 W   0.5 W   1.0 W

OVX-BD + rESW
1 bar   2 bar   3 bar

OVX-BD + ES
8 mA   16 mA

C

BV/TV (%)

OVX-BD   0.05 W   0.5 W   1.0 W   1 bar   2 bar   3 bar   8 mA   16 mA

OVX-BD + US   OVX-BD + rESW   OVX-BD + ES
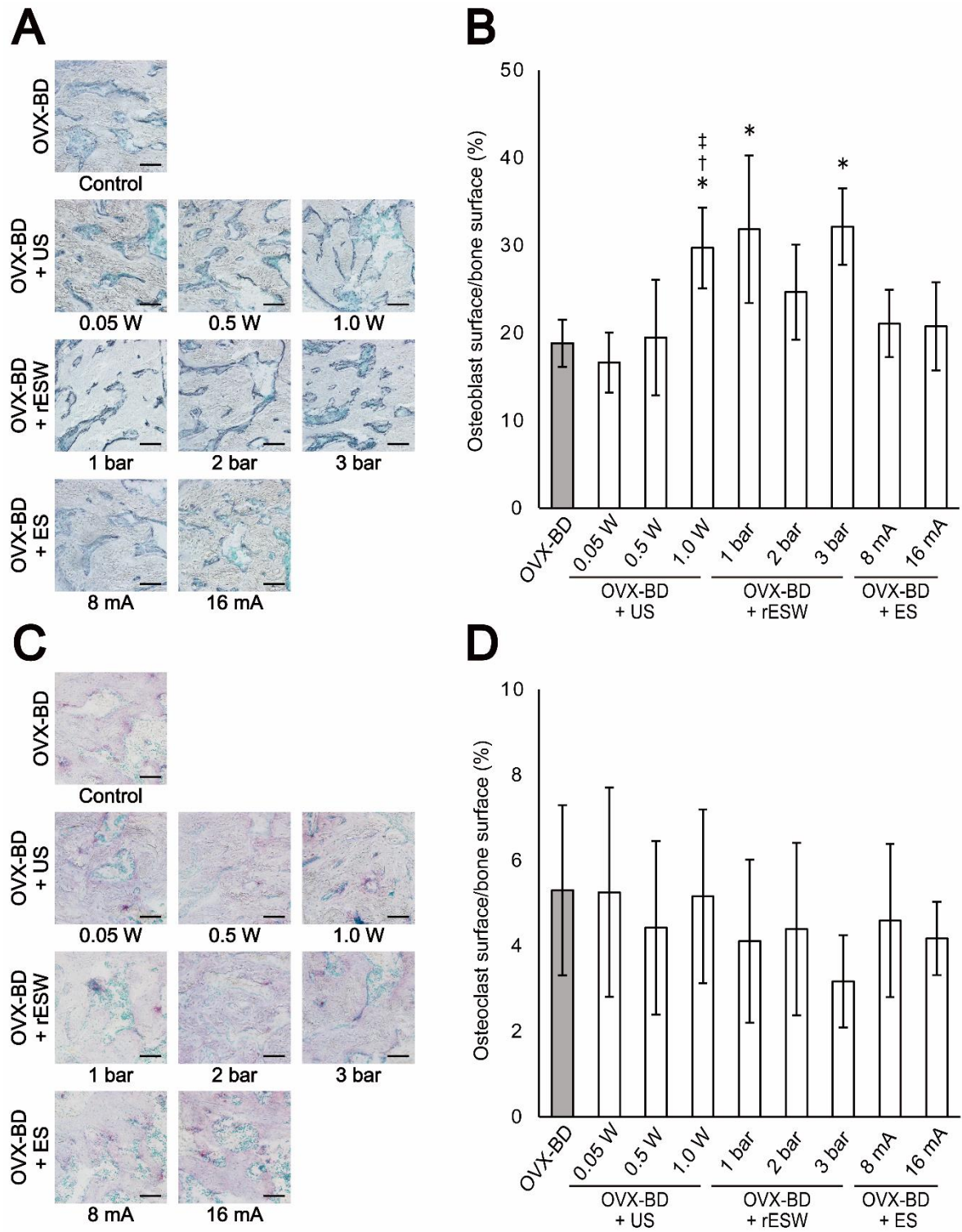
D

OVX-BD

OVX-BD + rESW

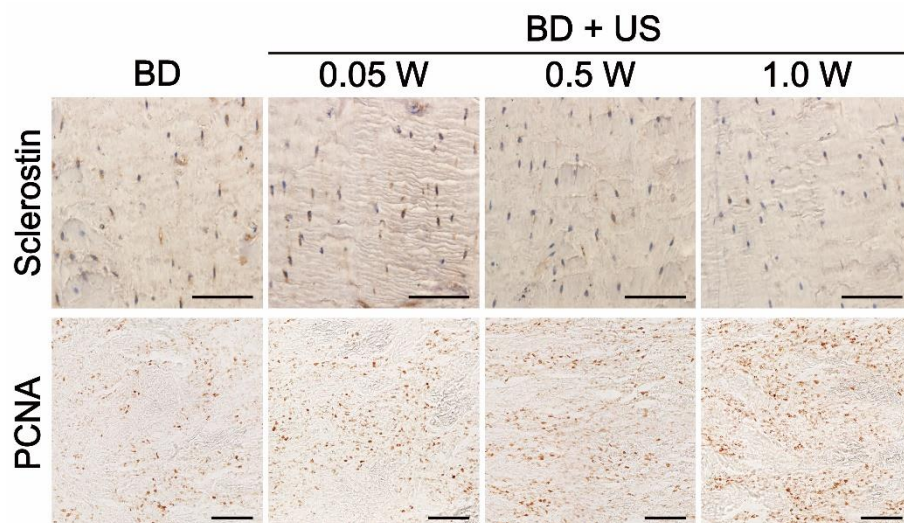Figure 3

Figure 4

Figure 5

Figure 6

Table 1. Maximum load of newly formed bone in defect sites determined by mechanical testing.

Group	BD	BD + US			OVX-BD	OVX-BD + US			OVX-BD + rESW			OVX-BD + ES	
		0.05 W/cm^2	0.5 W/cm^2	1.0 W/cm^2		0.05 W/cm^2	0.5 W/cm^2	1.0 W/cm^2	1 bar	2 bar	3 bar	8 mA	16mA
Maximum load (N)	20.7 ± 5.4	34.9 ± 8.9	27.6 ± 15.0	33.2 ± 7.5	34.0 ± 6.3	31.1 ± 12.0	40.8 ± 9.2	45.2 ± 9.6	—	—	—	29.1 ± 10.6	25.2 ± 10.5

Data are expressed as mean ± SD. OVX = ovariectomy; BD = bone defect; US = ultrasound; rESW = radial extracorporeal shock wave; ES = electrical

stimulation

Table 2. Quantification of immunohistochemistry for sclerostin and PCNA.

Group	BD	BD + US			OVX-BD	OVX-BD + US			OVX-BD + rESW			OVX-BD + ES	
		0.05 W/cm²	0.5 W/cm²	1.0 W/cm²		0.05 W/cm²	0.5 W/cm²	1.0 W/cm²	1 bar	2 bar	3 bar	8 mA	16mA
Sclerostin-positive osteocytes (%)	74.2 ± 10.6	68.8 ± 9.5	54.2 ± 19.0	47.1 ± 3.9**	60.4 ± 7.8	52.3 ± 11.6	41.7 ± 10.0	$37.4 \pm 6.8^{\dagger}$	$40.7 \pm 12.5^{\dagger}$	$36.8 \pm 4.8^{\dagger}$	$40.2 \pm 11.8^{\dagger}$	50.2 ± 12.6	48.9 ± 7.1
PCNA-positive cells (/10^5 µm²)	17.4 ± 4.1	23.9 ± 5.7	40.2 ± 10.4*	40.6 ± 2.7*	−	−	−	−	−	−	−	−	−

Data are expressed as mean ± SD. *$P < 0.05$ vs. BD group; **$P < 0.10$ vs. BD group; †$P < 0.05$ vs. OVX-BD group. OVX = ovariectomy; BD = bone defect;

US = ultrasound; rESW = radial extracorporeal shock wave; ES = electrical stimulation

Supplementary Table 1. Trabecular microarchitecture of the diaphyseal defect in normal rats quantified by μCT.

Group	BD	BD + US			BD + rESW			BD + ES	
		0.05 W/cm^2	0.5 W/cm^2	1.0 W/cm^2	1 bar	2 bar	4 bar	8 mA	16 mA
Tb.N (1/μm)	1.2 ± 0.4	1.7 ± 0.2	2.0 ± 0.4*	1.8 ± 0.2	1.4 ± 0.7	1.0 ± 0.3	1.1 ± 0.3	1.5 ± 0.4	1.8 ± 0.3
Tb.Th (μm)	126.0 ± 46.9	103.8 ± 9.6	100.1 ± 22.2	84.6 ± 15.2	108.2 ± 28.9	121.1 ± 20.8	137.2 ± 9.5	109.4 ± 14.8	101.6 ± 4.0
Tb.Sp (μm)	46.9 ± 1.5	47.8 ± 3.2	50.7 ± 5.3	51.2 ± 4.2	45.9 ± 6.8	45.4 ± 2.1	44.1 ± 3.8	42.2 ± 0.3	45.4 ± 3.6

Data are expressed as mean ± SD. *$P < 0.05$ vs. BD group. BD = bone defect; US = ultrasound; rESW = radial extracorporeal shock wave; ES = electrical stimulation; Tb.N = trabecular bone number; Tb.Th = trabecular bone thickness; Tb.Sp = trabecular bone separation

Supplementary Table 2. Trabecular microarchitecture of the metaphyseal defect in osteoporotic rats quantified by μCT.

Group	OVX-BD	OVX-BD + US			OVX-BD + rESW			OVX-BD + ES	
		0.05 W/cm^2	0.5 W/cm^2	1.0 W/cm^2	1 bar	2 bar	3 bar	8 mA	16 mA
Tb.N (1/μm)	3.5 ± 0.3	3.4 ± 0.3	4.7 ± 0.6*†	4.4 ± 0.5*†	4.0 ± 0.2	4.4 ± 0.6*	4.2 ± 0.5	4.5 ± 1.0	4.1 ± 0.8
Tb.Th (μm)	126.7 ± 9.2	141.1 ± 35.6	125.9 ± 8.0	137.6 ± 14.8	196.1 ± 34.5*	170.3 ± 45.7	215.5 ± 18.2*	117.1 ± 19.2	125.0 ± 45.4
Tb.Sp (μm)	142.3 ± 21.1	159.1 ± 37.7	95.7 ± 26.6	108.4 ± 51.4	55.9 ± 31.3*	60.3 ± 52.7*	23.7 ± 20.0*	112.2 ± 44.6	125.9 ± 41.9

Data are expressed as mean ± SD. *$P < 0.05$ vs. OVX-BD group; †$P < 0.05$ vs. OVX-BD + US at 0.05 W/cm^2 group. OVX = ovariectomy; BD = bone defect;

US = ultrasound; rESW = radial extracorporeal shock wave; ES = electrical stimulation; Tb.N = trabecular bone number; Tb.Th = trabecular bone thickness;

Tb.Sp = trabecular bone separation